Formation and properties of strontium-based bulk metallic glasses with ultralow glass transition temperature

Kun Zhao[a)]
Institute of Physics, Chinese Academy of Sciences, Beijing 100190, People's Republic of China; and Hebei University of Science and Technology, Shijiazhuang 050018, People's Republic of China

Wei Jiao, Jiang Ma, Xuan Qiao Gao, and Wei Hua Wang
Institute of Physics, Chinese Academy of Sciences, Beijing 100190, People's Republic of China

(Received 13 January 2012; accepted 31 May 2012)

We report a family of novel Strontium (Sr)-based bulk metallic glasses (BMGs) with good glass-forming ability and ultralow glass transition temperature (T_g) by strategic composition design. The Sr-based BMGs can be easily formed with wide composition range by a conventional copper mold cast method. The glassy alloys have many unique and diversified properties such as lowest glass transition temperature, ultralow elastic modulus, small value of Poisson's ratio and fragility, homogeneous flow at room temperature and tunable water degradation behavior. The BMGs with novel physical and chemical properties could have potential applications for biomaterial and micromanufacture, and are model system for studying some fundamental issues such as crystallization, relaxation and deformation in metallic glass.

I. INTRODUCTION

Bulk metallic glasses (BMGs) have attracted much attention due to their considerable scientific importance and potential technical applications.[1–5] The glassy alloys show very high strength at ambient temperature and viscous flow above glass transition temperature (T_g). They are useful for fabricating microscale devices due to their excellent characteristics such as high strength, isotropic homogeneity, freedom from grain boundary and good thermoplasticity.[6–9] The molding and imprinting for conventional metallic glasses have to be performed at high temperature. In contrast, the BMGs with low T_g shows polymer-like thermoplastic formability near room temperature, yet they show clearly metallic properties such as good thermal and electrical conductivity. Such materials with unique combination properties of metals and polymers can be regarded as metallic plastics.[10–12] They have potential in applications and can facilitate studies of some fundamental issues such as glass transition, slow dynamics in glass and supercooled liquid state. Therefore, the development of low-T_g BMGs is important for both scientists and engineers.

In this work, we report studies of the formation and properties of Sr-based BMGs with ultralow T_g by composition design based on elastic moduli criterion.[13] The newly developed Sr-based BMGs have low elastic constants and low glass transition temperature (26 °C, close to room temperature). Besides, the new alloys have other interesting properties such as small Poisson's ratio, strong liquids behavior in the framework of the fragility concept, tunable water degradation behavior, and room temperature homogeneous flow.

II. EXPERIMENTAL

The Sr-based BMGs with nominal compositions mentioned in this work were prepared by melting base element Sr (99%) with Zn (99.9%), Mg (99.9%), Cu (99.9%), Yb (99.5%), Ca (99%), and Mg–Li alloy (75 wt% Mg) using induction-melting method in a quartz tube under vacuum (better than 3.0×10^{-3} Pa). The melt was subsequently cast into the copper mold. All the compositions mentioned in this work can be cast in fully amorphous state at least 3 mm in diameter. The liquid nitrogen-cooled copper mold can enhance glass-forming ability (GFA) significantly. Their structure was examined by x-ray diffraction (XRD) using a MAC M03 diffractometer (Cu K_α radiation; Hiroshima, Japan). Differential scanning calorimetry (DSC) was performed under a purified argon atmosphere in a Mettler Toledo DSC822e (Schwerzenbach, Switzerland). The density ρ was measured by Archimedes' principle in absolute alcohol. The travel time of ultrasonic wave propagating through the sample was measured using a MATEC 6600 ultrasonic system (MATEC Inc., Northborough, MA) with a measuring sensitivity of 0.5 ns and a carrying frequency of 10 MHz. The physical properties (including the Young's modulus E, the shear modulus G, the bulk modulus B, Poisson's ratio ν, and Debye temperature θ_D) were derived from the acoustic

[a)]Address all correspondence to this author.
e-mail: zhk3415@163.com
DOI: 10.1557/jmr.2012.214

data and density. The compression specimens with gauge aspect ratio of 2:1 cut out of as-cast 2 mm rods were tested using Instron electromechanical testing system 3384 (Norwood, MA) at room temperature in air. The surface patterns of the samples were observed using scanning electron microscopy (SEM: Philips XL 30 instrument; Philips, Eindhoven, The Netherlands).

III. RESULTS AND DISCUSSIONS

A. Composition design

We develop Sr-based BMGs with ultralow glass transition temperature based on the elastic moduli criterion.[13–15] Extensive data on elastic moduli and T_g of BMGs exhibit that there is clear correlation between the elastic moduli and T_g. That is, the lower the value of elastic modulus of a BMG is, lower is the value of T_g. It is also found that the elastic constants M of BMGs show a correlation with a weighted average of the elastic constants M_i for the constituent elements as: $M^{-1} = \sum f_i \cdot M_i^{-1}$, where f_i denotes the atomic percentage of the constituent. The established correlation between elastic moduli and T_g is our guidelines for the development of the BMGs with much lower T_g by appropriate composition selection of components. Table I lists the shear modulus of Sr and other BMG base elements. Strontium has low elastic constants. Its shear modulus (G: 6.1 GPa) is even lower than that of cerium (Ce), calcium (Ca) and ytterbium (Yb) (The shear moduli of Ce, Ca, and Yb are 14, 7.4, and 9.9 GPa, respectively), which are typical metallic plastic base elements.[16] So the strontium is chosen as base element for developing the BMGs with low T_g.

Inoue's three empirical rules offer useful guideline for alloy design and have been used widely for developing new BMG compositions.[2] Deep eutectic is another empirical rule, which was used widely for developing new metallic glasses.[17] Table I lists the heat of mixing, atomic radius, and eutectic temperature of other components with strontium. For simplicity's sake, only elements, which have negative heat of mixing with Sr, are given. Strontium has large atomic radius and significantly different atomic size with listed elements. All the elements listed meet the requirements of Inoue's empirical rules. Zinc has the deepest eutectic with strontium, and the eutectic temperature is only 369 °C, so, zinc is chosen as one of the doping elements. Magnesium is chosen as another doping element because it has significantly different atomic size ratio with both Sr and Zn, and Mg also has deep eutectic with Sr.

TABLE I. Heat of mixing, atomic size and eutectic temperature of elements with strontium.

Elements	Heat of mixing (kJ/mol)	Atomic size (pm)	Eutectic temperature (°C)
Sr	...	215.1	...
Be	−10	111.3	...
Na	−2	185.8	...
Mg	−4	160	426
Al	−18	143.1	590
Ni	−1	124.6	660
Cu	−9	127.8	507
Zn	−21	133.2	369
Ga	−27	122.1	503
Pd	−84	137.6	...
Ag	−29	144.4	436
Sn	−46	140.5	745
Pt	−83	137.6	670
Au	−74	144.4	520
Bi	−61	154.7	658

Figure 1(a) shows XRD pattern of the as-cast $Sr_{60}Mg_{18}Zn_{22}$ alloy. The broad diffraction peaks without any clearly sharp diffraction peaks corresponding to crystalline phases indicate that the as-cast sample is in amorphous state within the detectable limit of the XRD, although there could be some crystalline phase (less than 5%) in it. Figure 1(b) presents the DSC trace of the as-cast $Sr_{60}Mg_{18}Zn_{22}$ BMG, and the heating rate is 10 K/min. It can be seen that an obvious endothermic characteristic of the glass transition followed by crystallization peaks is exhibited. The distinctive glass transition and sharp crystallization event confirmed the glassy state. The endothermic peak corresponds to the melting of the alloy. The shape of the melting peak indicates that the alloy is close to the eutectic point, which is one of the reasons behind its good GFA.

It is notable that the purity of Sr element is 99% (atomic percent). Inclusions or dissolved impurities in the melt are one of the important extrinsic factors, for they may influence the heterogeneous nucleation during solidification.[18] The impurities might affect the reproducibility of the results.

B. Composition range

Minor addition provides a powerful tool for the BMG-forming alloys development and design.[19] The GFA and properties of the BMGs are quite sensitive to the composition, and the addition technique has already played an

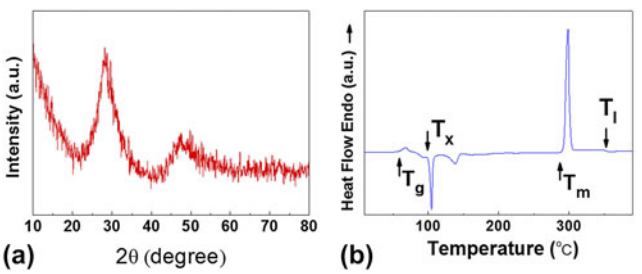

FIG. 1. (a) XRD pattern of the as-cast $Sr_{60}Mg_{18}Zn_{22}$ BMG. (b) DSC curve of the as-cast $Sr_{60}Mg_{18}Zn_{22}$ BMG.

effective and important role in GFA, improvement of thermal stability and properties of BMGs since the advent of BMGs. The addition method is applied to explore new Sr-based BMGs composition. Yb, Ca, Li, and Cu can be doped into the Sr-based BMG to improve the properties of the alloy. For example, the Yb can significantly enhance the corrosion resistance of the alloy, while Li addition can further lower the T_g of the alloy. Figure 2 shows the XRD patterns of the Sr-based BMGs with different additions. The broad diffraction peaks without appreciable sharp crystalline peaks in the XRD curves indicate the full amorphous phase of these alloys.

A topological structural model has been developed recently to interpret the composition of the BMG-forming alloys.[20–22] Amorphization occurs when local atomic strains generated by size differences between solute and solvent elements attain a critical level. It is supposed that the solute occupies substitutional lattice site in the crystalline lattice of the solvent element. In this case, the critical level of lattice instability is achieved at a lower concentration of a solute element as the difference in atomic size between the solvent and the solute elements increased. However, as the solute atom becomes increasingly smaller relative to the solvent atom, a substitutional occupancy is no longer stable and the smaller solute atoms may occupy alternate sites in the crystalline lattice, such as interstices. For Sr-based BMGs, the solute elements (Li, Mg, Zn, and Cu) are smaller than the solvent atoms (Sr, Ca, and Yb), so the interstitial atoms produce a positive lattice strain and the substitutional atoms create a negative lattice strain. In this case, the concentration of the substitutional atoms (Li and Mg) is the least in the glass-forming alloy, while the concentration of interstitial atoms (Zn and Cu) increases a little. The Sr-based BMGs can be described by the formula:

$$(\mathbf{Sr}, \mathrm{Ca}, \mathrm{Yb})_A(\mathrm{Li}, \mathrm{Mg})_B(\mathrm{Zn}, \mathrm{Cu})_C \quad , \qquad (1)$$

with $A = 40$ to 70, $B = 5$ to 25, $C = 10$ to 35, and $A + B + C = 100$. A strong topological basis exists for the compositions represented in Eq. (1).[23] The concentration of the elements and their atomic size are consistent with the densely packed solute-centered cluster model proposed by Miracle et al. Such atomic-concentration arrangement in the Sr-based BMGs provides efficient atomic cluster packing, and this may be another reason why the Sr-based BMGs are good glass-formers.

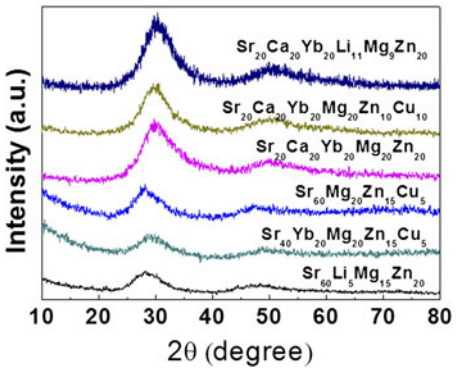

FIG. 2. XRD patterns of Sr-based BMGs.

C. Fragility

The fragility concept, as introduced by Angell, describes the different temperature dependencies of viscosity.[24] The change in viscosity or relaxation time reflects an intrinsic property of glass-forming liquids, and classifies liquids between two extremes: the strong extreme, where viscosity and relaxation time behave in an Arrhenius fashion with respect to temperature; and the fragile extreme, where these properties tend toward more non-Arrhenius behavior.[25] Metallic glasses display intermediate or strong fragility strength, as indicated by the fragility parameter, m.[26] From the Vogel–Fulcher–Tammann (VFT) fit, the m at a particular T_g can be calculated from[27]

$$m = \frac{DT_0T_g}{(T_g - T_0)^2 \ln 10} \quad , \qquad (2)$$

where D and T_0 are fitting parameters derived from VFT equation.

Figure 3(a) shows the DSC curves of the $Sr_{60}Mg_{18}Zn_{22}$ glass with heating rate over three orders of magnitude. The heating rates were 2, 5, 10, 20, 40, 80, 120, and 160 K/min, respectively. The corresponding glass transition temperatures were 332, 328, 331, 336, 341 K, 347, 349, and 352 K, respectively. A functional form of VFT type, which is suitable for fitting the present results, is[28]

$$\ln \phi = \ln B - \frac{DT_0}{T_g - T_0} \quad , \qquad (3)$$

where ϕ is the heating rate, and T_g is the glass transition temperature. B, D, and T_0 are adjustable parameters. From the VFT fit [Fig. 3(b)], D and T_0 of $Sr_{60}Mg_{18}Zn_{22}$ are determined to be 12.4 and 205 K, respectively. When the heating rate is 20 K/min, the glass transition temperature T_g is 336 K. The value m calculated from Eq. (2) is 21. It can be classified to the strong liquids in the framework of fragility, and the value m is smaller than other common BMGs such as Zr- ($m \sim 34$–39), Fe- ($m \sim 32$–37), Mg- ($m \sim 39$–46), and RE- ($m \sim 21$–53) based BMGs.[27,29–34] It is notable that some values of m are not determined from some of these methods, and it may cause some discrepancy.

It has been reported that the fragility of metallic glass is correlated with the number of components in the alloy.[35] In most cases, the metallic glass-forming liquids become stronger with increase in the number of elements. Metallic glass ribbons with two or three elements are more fragile

compared with BMGs with three or more elements.[30] The value m of the new developed $Sr_{60}Mg_{18}Zn_{22}$ alloy indicates that the Sr-based glass-forming liquids are rather strong. If more elements are added to the alloy, even stronger liquids are to be expected. The metallic glass-forming system is one of the simplest systems where the microstructure units are composed of metallic atoms. The strong metallic glass-forming liquid may facilitate the study of some fundamental issues such as glass transition and relaxation in glass.

High-mixing entropy is a new route for designing novel BMGs.[36,37] The $Sr_{20}Ca_{20}Yb_{20}Mg_{20}Zn_{20}$ alloy was determined from the prototype $Sr_{60}Mg_{18}Zn_{22}$ BMG in accordance with strategic alloy design. The fragility of $Sr_{20}Ca_{20}Yb_{20}Mg_{20}Zn_{20}$ BMG was determined using the same method as used for $Sr_{60}Mg_{18}Zn_{22}$. The adjustable parameters D and T_0 were 107 and 80.6 K, respectively. The fragility index m was 17 calculated from Eq. (2) (T_g = 357 K, heating rate 20 K/min). It is the lowest value recorded among known metallic glasses.

D. Low elastic constant and low glass transition temperature

The longitudinal (v_l) and transverse (v_s) velocities, densities, elastic constants, Poisson's ratio, and Debye temperature of Sr-based BMGs are listed in Table II. The Sr-based BMGs have relatively low density ($\rho \sim 3.5$ g/cm^3). The density of Sr-based BMGs is just higher than that of Ca-based BMGs,[23] but much lower than other conventional BMGs such as Zr-, Cu-, and Pd-based BMGs.[13] The Sr-based BMGs have the lowest elastic constant among all the known BMGs. For $Sr_{20}Ca_{20}Yb_{20}Li_{11}Mg_9Zn_{20}$ BMG, the Young's modulus is as low as 16.1 GPa, which is comparable to the human bone (2–18 GPa). The Sr-based BMGs have small value for Poisson's ratio. For $Sr_{60}Mg_{18}Zn_{22}$, the Poisson's ratio ν is just 0.276. Brittleness is expected in metallic glasses with smaller values of Poisson's ratio.[38] However, due to the low glass transition temperature, uncommon room temperature rheology is observed. The Sr-based BMGs have low Debye temperature θ_D. Debye temperature is indicative of the relative strength of the atomic bond. The low Debye temperature implies weak bonding of the alloy atoms, which is consistent with the low elastic constants.[13]

The thermodynamic parameters of Sr-based BMGs derived from DSC curves are listed in Table III. The BMGs have the lowest glass transition temperature among all the known BMGs. For $Sr_{60}Li_{11}Mg_9Zn_{20}$, the T_g is just 26 °C, which is at room temperature. However, due to the ultralow T_g, it is unstable at room temperature. It begins to crystallize at about 1 h after being cast, and will achieve fully crystallized phase in 24 h as indicated by x-ray diffraction. The $Sr_{60}Li_5Mg_{15}Zn_{20}$ with a little higher T_g (42 °C) is much more stable. It remains in amorphous state after 1 wk at room temperature. The Sr-based BMGs was designed by elastic correlations, which also confirm the elastic criterion well. The Li (Young's modulus E: 4.9 GPa) have the lowest elastic moduli among all BMG-forming elements. The glass transition temperature can be tuned by Li content (Fig. 4). As the Li content increases, the T_g of the BMGs shifts to lower temperature, and finally reaches to room temperature.

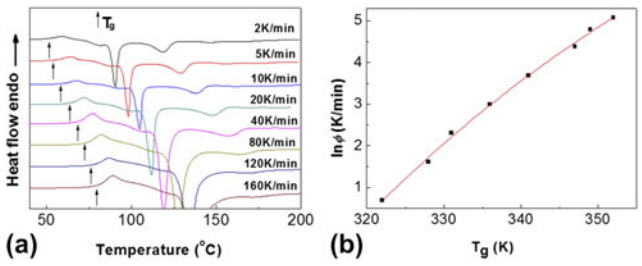

FIG. 3. (a) DSC curves of $Sr_{60}Mg_{18}Zn_{22}$ BMG at different heating rate and (b) VFT relation between glass transition temperature T_g and heating rate φ of $Sr_{60}Mg_{18}Zn_{22}$ BMG.

E. Room temperature rheology

We note that brittleness is expected in metallic glasses with small values of Poisson's ratio or large values of the ratio of shear modulus to bulk modulus.[38] The Poisson's ratio is regarded as indicator of the plastic character for BMGs and this idea was verified in various BMGs. The Sr-based BMGs have small Poisson's ratio, and it should be attributed to the class of brittle BMGs. However, the BMG could show superplasticity at room temperature due to the ultralow T_g. It is well known that the deformation behavior of metallic glasses scales with glass transition temperature T_g. The transition from

TABLE II. Acoustic velocity, density, elastic constant, Poisson's ratio, and Debye temperature of Sr-based BMGs.

Composition	V_s (km/s)	V_l (km/s)	ρ (g/cm^3)	E (GPa)	G (GPa)	B (GPa)	ν	θ_D (K)
$Sr_{60}Mg_{18}Zn_{22}$	1.592	2.862	3.04	19.7	7.71	14.6	0.276	156
$Sr_{60}Mg_{20}Zn_{15}Cu_5$	1.598	2.905	3.04	19.9	7.76	15.3	0.283	157
$Sr_{40}Yb_{20}Mg_{20}Zn_{15}Cu_5$	1.413	2.668	3.95	20.6	7.88	17.6	0.305	142
$Sr_{20}Ca_{20}Yb_{20}Mg_{20}Zn_{20}$	1.580	2.872	3.56	22.8	8.89	17.5	0.283	158
$Sr_{20}Ca_{20}Yb_{20}Mg_{20}Zn_{10}Cu_{10}$	1.316	2.394	3.71	24.3	9.47	18.6	0.282	162
$Sr_{60}Li_5Mg_{15}Zn_{20}$	1.531	2.918	2.99	18.4	7.02	16.1	0.310	151
$Sr_{20}Ca_{20}Yb_{20}Li$	2.244	3.919	3.63	16.1	6.28	12.4	0.283	134

TABLE III. Thermodynamic parameters of Sr-based BMGs.

Composition	T_g (°C)	T_x (°C)	T_m (°C)	T_l (°C)	T_{rg}
$Sr_{60}Mg_{18}Zn_{22}$	58	101	291	353	0.53
$Sr_{60}Li_{11}Mg_9Zn_{20}$	26	50	236	276	0.54
$Sr_{60}Li_5Mg_{15}Zn_{20}$	42	63	255	300	0.55
$Sr_{60}Mg_{20}Zn_{15}Cu_5$	62	101	293	332	0.55
$Sr_{40}Yb_{20}Mg_{20}Zn_{15}Cu_5$	63	105	327	360	0.53
$Sr_{20}Yb_{20}Ca_{20}Mg_{20}Zn_{20}$	80	116	285	357	0.56
$Sr_{20}Yb_{20}Ca_{20}Mg_{20}Zn_{10}Cu_{10}$	78	118	288	369	0.55
$Sr_{20}Yb_{20}Ca_{20}Li_{11}Mg_9Zn_{20}$	46	71	247	286	0.57

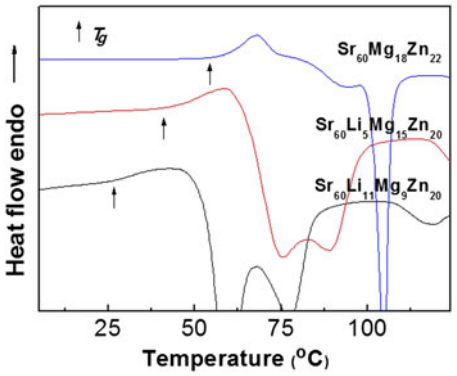

FIG. 4. DSC curves of Sr-based BMGs with different Li content.

inhomogeneous to homogeneous flow occurs at approximately 0.8 T/T_g. For this alloy, room temperature lies within the homogeneous flow regime (T/T_g = 0.93). Figure 5 shows the imprinted pattern on the BMGs. The BMG was under a pressure of 50 MPa for 24 h, and the smooth surface emerged as square array. The imprinting for other BMGs is usually carried out in the supercooled liquid region with much higher temperature, but this BMG can be imprinted at room temperature. The polymer-like thermoplastic behavior is convenient for micro- and nanomanufacture.[6,39]

Figure 6(a) shows the stress–strain curves of the $Sr_{20}Ca_{20}Yb_{20}Li_{11}Mg_9Zn_{20}$ BMG. When the strain rate is 1×10^{-3} /s, the sample breaks into pieces just after elastic deformation, which resembles Mg- and Ca-based BMGs.[40,41] The inset on the left shows the SEM image of the pieces. However, when the strain rate decreases to a slightly lower value of 1×10^{-4} /s, the BMG exhibits a complete change in deformation behavior. It shows elastic strain limit of ~2% before yielding, and then displays superplasticity as observed in the supercooled liquid state for other BMGs.[42–44] The sample can be compressed to 70% of its original height without cracking, and further compression is still possible to extend the deformation. The XRD examination verifies that the severe deformed sample remains fully amorphous state. The scanning electron microscopy (SEM) shows that the severe deformed specimen keeps smooth surface. No

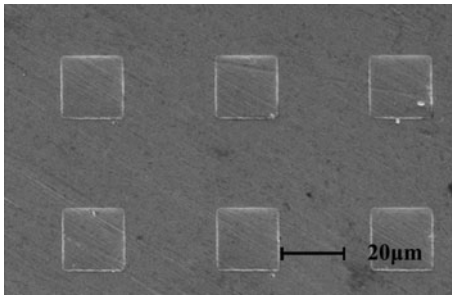

FIG. 5. SEM image of square array on the surface of Sr-based BMG imprinted at room temperature.

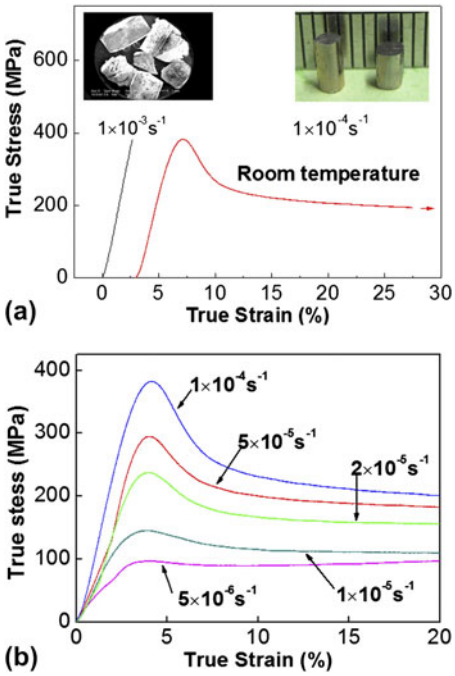

FIG. 6. (a) Different deformation type of $Sr_{20}Ca_{20}Yb_{20}Li_{11}Mg_9Zn_{20}$ BMG at room temperature. The inset at left shows that the BMG is brittle at high strain rate, while the inset at right shows that the BMG is superplastic at low strain rate. (b) Stress–strain curves of $Sr_{20}Ca_{20}Yb_{20}Li_{11}Mg_9Zn_{20}$ BMG at different strain rate.

primary shear band and other observable shear bands can be found, which confirms the uniform deformation and homogeneous flow of metallic glass at room temperature.[45]

For homogeneous flow in metallic glass, the flow stress changes with different strain rate. Figure 6(b) shows the stress–strain curves of the $Sr_{20}Ca_{20}Yb_{20}Li_{11}Mg_9Zn_{20}$ with wide strain rate region. The yield stress and steady flow stress increase with strain rate. It belongs to Non-Newtonian fluid, which is the characteristic of BMG for homogeneous deformation. The compression behavior of this BMG can be expressed by free volume theory. Spaepen gives the stress–strain relation in metallic glass based on free volume theory. The original equation is written in shear stress and shear strain rate.[46] For normal stress and normal strain rate, the equation changes to [47]:

$$\dot{\varepsilon} = 2c_f v_D \exp\left(-\frac{\Delta G^m}{kT}\right) \sinh\left(\frac{\sigma V}{2\sqrt{3}kT}\right) \quad , \quad (4)$$

where $\dot{\varepsilon}$ is the normal strain rate, c_f is the concentration of defect, v_D is the Debye frequency, ΔG^m is the activation free energy migration, σ is the normal stress, and V is the activation volume.

The experiments were carried out at room temperature. If relatively small variation of the flow defect concentration with strain is assumed, the defect concentration depends only on temperature. Since the experiments were carried out near the glass transition temperature for long duration, the defect concentration when deformation starts is supposed to be equal to its equilibrium value.[47] In such a framework, Eq. (4) can be rewritten:

$$\dot{\varepsilon} = \dot{\varepsilon}_0 \sinh(a\sigma) \quad , \quad (5)$$

where $\dot{\varepsilon}_0 = 2c_f v_D \exp\left(-\frac{\Delta G^m}{kT}\right)$ and $a = \frac{V}{kT}$. Both of them are constant based on the supposition above.

The strain rate and the maximum flow stress follow Eq. (5). At low strain rate, the maximum flow stress grows with strain rate. However, the maximum flow stress will not exceed the fracture stress, which is regarded as the intrinsic character of BMGs at strain rate covering the entire quasistatic range.[48] When the maximum flow stress reaches fracture stress (for this BMG, the critical strain rate is 1×10^{-3} /s and the critical stress is 400 MPa as indicated by experiment), the sample breaks into pieces. The deformation behavior of the Sr-based BMGs changes at a critical strain rate, and the transition from homogeneous deformation to inhomogeneous deformation occurs.

F. Corrosion behavior

Strontium is friendly to human body, and it is useful for the treatment and prevention of osteoporosis. However, crystalline Sr is extremely reactive. It reacts with water strongly. The reaction gives a lot of heat, and produces large amounts of gas. Metallic glasses usually have much more desirable corrosion resistance than their crystalline counterparts.[49] Mg- and Ca-based BMGs glasses are regarded as promising biodegradable materials.[4,50,51] Strontium-based BMGs constitute a new class of alkaline earth-based BMGs. The stability of Sr-based BMGs in aqueous environment determines whether the material is suitable for biodegradable application.

The water degradation of Sr-based BMGs in water can be modulated by minor addition. Figure 7(a) shows the weight change of Sr-based BMGs in deionized water, where m_0 represents the original alloy weight, and m represents the weight that the alloy has been immersed in water for some time. For Yb-free Sr-based BMGs, bubbles are produced immediately after the BMGs are immersed in water. The solid alloys dissolved in water in less than

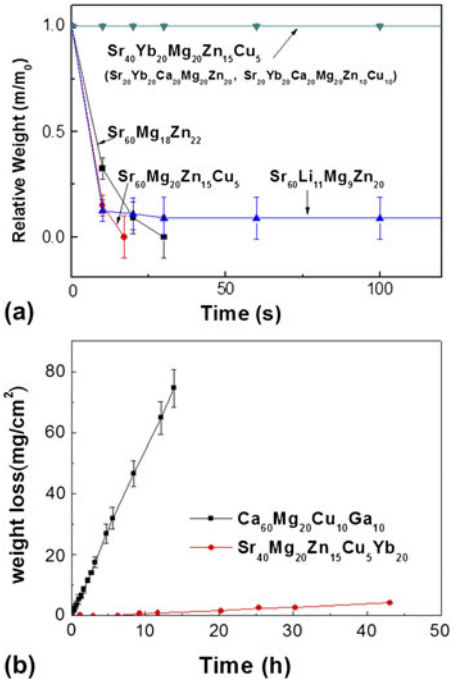

FIG. 7. (a) Weight change of Sr-based BMGs in deionized water. (b) Weight loss of $Sr_{40}Mg_{20}Zn_{15}Cu_5Yb_{20}$ and $Ca_{60}Mg_{20}Cu_{10}Ga_{10}$ BMGs in Hanks solution.

1 min and the water became muddy black due to the violent reaction.[52] The Yb-doped Sr-based BMGs show totally different behavior in water. They are much more stable than the Yb-free ones in deionized water. They could stay in water for more than a week without observable weight change.

Hanks solution is a salt solution usually used as simulated body fluids. The degradation behavior of Sr-based BMG in Hanks solution can help us to evaluate the feasibility of it as biodegradable materials. Figure 7(b) shows the weight loss of Sr- and Ca-based BMGs in Hanks solution. The weight loss of the $Sr_{40}Yb_{20}Mg_{20}Zn_{15}Cu_5$ BMG in Hanks solution is much slower than the Ca-based BMG. The slowdown degradation in Hanks solution is favorable for biodegradation materials. Fast degradation rate is harmful to human body because the degradation process is usually accompanied with hydrogen evolution, and it is not conducive for the functional requirement of the human body. The Yb-doped Sr-based BMGs might be potential biodegradation materials, and further studies are needed to prove the supposition.

IV. CONCLUSIONS

We report a class of Sr-based BMGs, which have extremely low glass transition temperature approaching room temperature, good GFA in a wide composition range and strong liquid behavior. Due to the ultralow T_g, the Sr-based BMG shows room temperature homogeneous

flow just as other BMGs behave in supercooled liquid region at high temperature. The Sr-based BMGs also have tunable water degradation behavior. The Sr-based BMGs have potential applications and are also model system for scientific issues in glass physics.

ACKNOWLEDGMENTS

Financial support from NSF of China (50921091 and 50731008) and MOST973 of China (2007CB613904 and 2010CB731603) is greatly appreciated. Experimental aid of H.B. Ke, and T. Wang is acknowledged. The provision of Mg-Li master alloy by Prof. M.L. Zhang is acknowledged.

REFERENCES

1. A.L. Greer: Metallic glasses… on the threshold. *Mater. Today* **12**,14 (2009).
2. A. Inoue: Stabilization of metallic supercooled liquid and bulk amorphous alloys. *Acta Mater.* **48**, 279 (2000).
3. W.L. Johnson, G. Kaltenboeck, M.D. Demetriou, J.P. Schramm, X. Liu, D. Samwer, C.P. Kim, and D.C. Hofmann: Beating crystallization in glass-forming metals by millisecond heating and processing. *Science* **332**, 828 (2011).
4. B. Zberg, P.J. Uggowitzer, and J.L. Löffler: MgZnCa glasses without clinically observable hydrogen evolution for biodegradable implants. *Nat. Mater.* **8**, 887 (2009).
5. S. Pauly, S. Gorantla, S.G. Wang, U. Kühn, and J. Eckert: Transformation-mediated ductility in CuZr-based bulk metallic glasses. *Nat. Mater.* **7**, 473 (2010).
6. G. Kumar, H.X. Tang, and J. Schroers: Nanomolding with amorphous metals. *Nature* **457**, 868 (2009).
7. Y. Saotome, K. Itoh, T. Zhang, and A. Inoue: Superplastic nanoforming of Pd-based amorphous alloy. *Scr. Mater.* **44**, 1541 (2001).
8. J.P. Chu, H. Wijaya, C.W. Wu, T.R. Tsai, C.S. Wei, T.G. Nier, and J. Wadsworth: Nanoimprinting of gratings on a bulk metallic glass. *Appl. Phys. Lett.* **90**, 034101 (2007).
9. C.T. Pan, T.T. Wu, M.F. Chen, Y.C. Chang, C.J. Lee, and J.C. Huang: Hot embossing of microlens array on bulk metallic glass. *Sens. Actuators, A* **141**, 422 (2008).
10. B. Zhang, D.Q. Zhao, M.X. Pan, W.H. Wang, and A.L. Greer: Amorphous metallic plastic. *Phys. Rev. Lett.* **94**, 205502 (2005).
11. J.F. Li, D.Q. Zhao, M.L. Zhang, and W.H. Wang: CaLi-based bulk metallic glasses with multiple superior properties. *Appl. Phys. Lett.* **93**, 171907 (2008).
12. W. Zhang, H. Guo, M.W. Chen, Y. Saotome, C.L. Qin, and A. Inoue: New Au-based bulk glasses alloys with ultralow glass transition temperature. *Scr. Mater.* **61**, 744 (2009).
13. W.H. Wang: Correlations between elastic moduli and properties in bulk metallic glasses. *J. Appl. Phys.* **99**, 093506 (2006).
14. W.H. Wang: Elastic moduli and behaviors of metallic glasses. *J. Non-Cryst. Solids* **351**, 1481 (2005).
15. W.H. Wang: The elastic properties, elastic models and elastic perspectives of metallic glasses. *Prog. Mater. Sci.* **57**, 487 (2012).
16. J.F. Li, J.Q. Wang, X.F. Liu, K. Zhao, H.Y. Bai, M.X. Pan, and W.H. Wang: Glassy metallic plastic. *Sci. China Phys. Mech. Astron.* **53**, 409 (2010).
17. M.H. Cohen and D. Turnbull: Composition requirement for glass formation in metallic and ionic systems. *Nature* **189**, 131 (1961).
18. D.V. Louzguine-Luzgin, D.B. Miracle, and A. Inoue: Intrinsic and extrinsic factors influencing the glass-forming ability of alloys. *Adv. Eng. Mater.* **10**, 1008 (2008).
19. W.H. Wang: Roles of minor additions in formation and properties of bulk metallic glasses. *Prog. Mater Sci.* **52**, 540 (2007).
20. O.N. Senkov, D.B. Miracle, and H.M. Mullens: Topological criteria for amorphization based on a thermodynamic approach. *J. Appl. Phys.* **97**, 103502 (2005).
21. D.B. Miracle: A structural model for metallic glasses. *Nat. Mater.* **3**, 697 (2004).
22. D.B. Miracle: The efficient cluster-packing model – An atomic structural model for metallic glasses. *Acta Mater.* **54**, 4317 (2006).
23. O.N. Senkov, D.B. Miracle, V. Keppens, and P.K. Liaw: Development and characterization of low-density Ca-based bulk metallic glasses: An overview. *Metall. Mater. Trans. A* **39**, 1888 (2008).
24. C.A. Angell: Relaxation in liquids, polymers and plastic crystals – strong/fragile patterns and problems. *J. Non-Cryst. Solids* **131–133**, 13 (1991).
25. Z. Evenson, I. Gallino, and R. Busch: The effect of cooling rates on the apparent fragility of Zr-based bulk metallic glasses. *J. Appl. Phys.* **107**, 123529 (2010).
26. D.N. Penera: Compilation of the fragility parameters of several glass-forming metallic alloys. *J. Phys. Condens. Matter* **11**, 3807 (1999).
27. R. Böhmer, K.L. Ngai, C.A. Angell, and D.J. Plazek: Nonexponential relaxations in strong and fragile glass formers. *J. Chem. Phys.* **99**, 4201 (1993).
28. R. Brüning and K. Samwer: Glass transition on long time scale. *Phys. Rev. B* **46**, 11318 (1992).
29. J.M. Borrego, A. Conde, S. Roth, and J. Eckert: Glass-forming ability and soft magnetic properties of FeCoSiAlGaPCB amorphous alloys. *J. Appl. Phys.* **92**, 2073 (2002).
30. E.S. Park, J.H. Na, and D.H. Kim: Correlation between fragility and glass-forming ability/plasticity in glass-forming alloys. *Appl. Phys. Lett.* **91**, 031907 (2007).
31. Z.F. Zhao, Z. Zhang, P. Wen, M.X. Pan. D.Q. Zhao, W.H. Wang and W.L. Wang: A high glass-forming alloy with low glass transition temperature. *Appl. Phys. Lett.* **82**, 4699 (2003).
32. B. Zhang, R.J. Wang, D.Q. Zhao, M.X. Pan, and W.H. Wang: Properties of Ce-based bulk metallic glass-forming alloys. *Phys. Rev. B* **70**, 224208 (2004).
33. Z. Zhang, W.H. Wang, and Y. Hirotsu: Glass-forming ability and crystallization behavior of $Nd_{60}Al_{10}Ni_{10}Cu_{20-x}Fe_x$ ($x = 0, 2, 4$) bulk metallic glass with distinct glass transition. *Mater. Sci. Eng., A* **385**, 38 (2004).
34. Q. Luo, D.Q. Zhao, M.X. Pan, R.J. Wang, and W.H. Wang: Hard and fragile holmium-based bulk metallic glasses. *Appl. Phys. Lett.* **88**, 181909 (2006).
35. L. Shadowspeaker and R. Busch: On the fragility of Nb-Ni-based and Zr-based bulk metallic glasses. *Appl. Phys. Lett.* **85**, 2508 (2004).
36. A. Takeuchi, N. Chen, T. Wada, Y. Yokoyama, H. Kato, A. Inoue, and J.W. Yeh: $Pd_{20}Pt_{20}Cu_{20}Ni_{20}P_{20}$ high-entropy alloy as a bulk metallic glass in the centimeter. *Intermetallics* **19**, 1546 (2011).
37. X.Q. Gao, K. Zhao, H.B. Ke, D.W. Ding, W.H. Wang, and H.Y. Bai: High-mixing entropy bulk metallic glasses. *J. Non-Cryst. Solids* **357**, 3557 (2011).
38. J.J. Lewandowski, W.H. Wang, and A.L. Greer: Intrinsic plasticity or brittleness of metallic glasses. *Philos. Mag. Lett.* **85**, 77 (2005).
39. G. Kumar and J. Schroers: Write and erase mechanisms for bulk metallic glass. *Appl. Phys. Lett.* **92**, 031901 (2008).
40. J.Q. Wang, P. Yu, and H.Y. Bai: Minor addition induced enhancement of strength of Mg-based bulk metallic glass. *J. Non-Cryst. Solids* **354**, 5440 (2008).

41. G.Y. Wang, P.K. Liaw, O.N. Senkov, D.B. Miracle, and M.L. Morrison: Mechanical and fatigue behavior of $Ca_{65}Mg_{15}Zn_{20}$ bulk-metallic glass. *Adv. Eng. Mater.* **11**, 27 (2009).
42. H. Kato, Y. Kawamura, A. Inoue, and H.S. Chen: Newtonian to non-Newtonian master flow curves of a bulk glass alloy $Pd_{40}Ni_{10}Cu_{30}P_{20}$. *Appl. Phys. Lett.* **73**, 3665 (1998).
43. J. Lu, G. Ravichandran, and W.L. Johnson: Deformation behavior of the ZrTiCuNiBe bulk metallic glass over a wide range of strain-rate and temperatures. *Acta Mater.* **51**, 3429 (2003).
44. J.S. Harmon, M.D. Demetriou, W.L. Johnson, and M. Tao: Deformation of glass-forming metallic liquids: Configurational changes and their relation to elastic softening. *Appl. Phys. Lett.* **90**, 131912 (2007).
45. K. Zhao, X.X. Xia, H.Y. Bai, D.Q. Zhao, and W.H. Wang: Room temperature homogeneous flow in a bulk metallic glass with low glass transition temperature. *Appl. Phys. Lett.* **98**, 141913 (2011).
46. F. Spaepen: A microscopic mechanism for steady state inhomogeneous flow in metallic glasses. *Acta Metall.* **25**, 407 (1977).
47. M. Bletry, P. Guyot, J.J. Blandin, and J.L. Soubeyroux: Free volume model: High-temperature deformation of a Zr-based bulk metallic glass. *Acta Mater.* **54**, 1257 (2006).
48. C.A. Schuh, T.C. Hufnage, and U. Ramamurty: Mechanical behavior of amorphous alloys. *Acta Mater.* **55**, 4067 (2007).
49. J. Dahlman, O.N. Senkov, J.M. Scott, and D.B. Miracle: Corrosion properties of Ca-based bulk metallic glasses. *Mater. Trans.* **48**, 1850 (2007)
50. X.N. Gu, Y.F. Zheng, S.P. Zhong, T.F. Xi, J.Q. Wang, and W.H. Wang: Corrosion of and cellular responses to Mg-Zn-Ca bulk metallic glasses. *Biomaterials* **31**, 1093 (2010).
51. Y.B. Wang, X.H. Xie, H.F. Li, X.L. Wang, M.Z. Zhao, E.W. Zhang, Y.J. Bai, Y.F. Zheng, and L. Qing: Biodegradable CaMgZn bulk metallic glass for potential skeletal application. *Acta Biomater.* **7**, 3196 (2011).
52. K. Zhao, J.F. Li, D.Q. Zhao, M.X. Pan, and W.H. Wang: Degradable Sr-based bulk metallic glasses. *Scr. Mater.* **61**, 1091 (2009).